Joint 3D deghosting of multiple vintages

Ping Wang, Jingbo Liu, Jeshurun Hembd, Suryadeep Ray (CGG)*

Summary

While most marine baseline surveys do not use broadband techniques, increasingly more monitor surveys are being adapted to broadband configurations that often use different receiver-depth profiles (e.g., deeper or variable-depth). A regular matching filter that has been commonly used in 4D time-lapse processing may be insufficient to normalize the wavelet difference between the baseline and monitor data because of the large difference in receiver-depth profiles. Deghosting can effectively remove the wavelet variation among vintages caused by different receiver depths. To take advantage of the potentially better spatial sampling from different surveys and possibly better overall signal-to-noise ratio (S/N) due to complementary ghost-notch frequencies, we propose a joint inversion scheme that uses both baseline and monitor data (or more vintages) that deghosts common events consistently while preserving the difference between vintages. Using synthetic and field data, we demonstrate that joint deghosting of baseline and monitor data provides a more accurate ghost removal and a more reliable 4D difference compared to separate deghosting of both data.

Introduction

Broadband processing that involves receiver deghosting (Kemal et al., 2008; Riyanti et al., 2008; Poole, 2013; Wang et al., 2014) and shot deghosting/designature (Van der Schans and Ziolkowski, 1983; Poole et al., 2013; Wang et al., 2015), and broadband surveys (Carlson et al., 2007; Robertsson et al., 2008; Soubaras, 2010) have been widely accepted as methods for extending the bandwidth of marine seismic data. Two questions have been frequently raised in the context of 4D time-lapse processing: (1) can we obtain deghosted 4D signals for broader bandwidth and (2) can we apply 4D processing between conventional surveys and broadband surveys? In an attempt to answer both questions, Hicks et al. (2014) demonstrated that deghosting was possible and important for 4D processing of multiple vintages with different receiver-depth profiles using a 2D ghost-wavefield elimination algorithm (Poole, 2013).

Wang et al. (2014) proposed using a progressive sparse Tau-P inversion algorithm for 3D deghosting of single-component marine seismic data. This algorithm was used to deghost both baseline and monitor data sets separately in 4D processing. To take advantage of the potentially better spatial sampling from different surveys (if receivers of two or more vintages are not perfectly collocated) and better overall S/N due to complementary ghost-notch frequencies (if receiver depths of two or more vintages are different), we extended this algorithm to perform joint 3D deghosting of multiple vintages.

Method

Sparse 3D Tau-P inversion has been proposed for 3D deghosting of marine seismic data (Wang et al., 2014). It was applied in the common-shot domain for marine towed-streamer data and in the common-node domain for ocean-bottom node (OBN) data. We focus on receiver deghosting of marine towed-streamer data unless specified.

The key to this 3D deghosting algorithm is to find a ghost-free $\tau - p_x - p_y$ model, U, at surface datum that best fits the recorded data, D, when reghosted and inverse $\tau - p_x - p_y$ transformed:

$$D(f; x^i, y^i, z^i) = \sum_j L(f; x^i, y^i; p_x^j, p_y^j) R(f; z^i; p_x^j, p_y^j) U(f; p_x^j, p_y^j), \quad (1)$$

where f is frequency, L is the reverse $\tau - p_x - p_y$ transform operator, R is the reghosting operator, (x^i, y^i, z^i) is the receiver location, and (p_x^j, p_y^j) is the slowness pair (i: trace index; j: slowness index). A fast Fourier transform (FFT) is applied to transform time, τ or t, into frequency, f. Next, we apply the reghosting and the reverse $\tau - p_x - p_y$ transform operators step-by-step.

First, in the $\tau - p_x - p_y$ domain, the ghost-delay time, T_i^j, can be written as a function of the receiver depth, z^i, the water velocity, v, and the slowness, (p_x^j, p_y^j):

$$T_i^j = 2z^i \sqrt{v^{-2} - (p_x^j)^2 - (p_y^j)^2}\,. \quad (2)$$

Once the ghost-delay time is known, we introduce a reghosting operator,

$$R(f; z^i; p_x^j, p_y^j) = e^{i\pi f T_i^j} - e^{-i\pi f T_i^j}. \quad (3)$$

The first term in Equation 3 redatums the ghost-free wavefield from surface datum to obtain the up-going wavefield at the cable datum; the second term generates the down-going wavefield (the receiver ghost) at the mirror cable datum and reverses the polarity.

The reverse $\tau - p_x - p_y$ transform operator can be written as a function of the horizontal receiver location, (x^i, y^i), and the slowness, (p_x^j, p_y^j):

$$L_j^i = e^{-i2\pi f (x^i p_x^j + y^i p_y^j)}. \quad (4)$$

Equation 1 can be simplified to matrix notion:

$$D = LRU. \quad (5)$$

In 4D time-lapse processing, we can apply Equation 5 to both baseline data, D_b, and monitor data, D_m, to remove the receiver ghost separately,

DOI http://dx.doi.org/10.1190/segam2015-5838448.1

$$\begin{cases} D_b = L^b R^b U_b \\ D_m = L^m R^m U_m \end{cases}, \quad (6)$$

where symbols with superscript or subscript b and m are for baseline and monitor data, respectively.

There are no interactions between the two deghosting inversions in Equation 6. To take advantage of the potentially better spatial sampling from both surveys and better overall S/N due to complementary ghost-notch frequencies, we modify the inversion scheme in Equation 6 to deghost the baseline and monitor data jointly,

$$\begin{pmatrix} D_b \\ D_m \end{pmatrix} = \begin{pmatrix} L^b R^b & L^b R^b & 0 \\ L^m R^m & 0 & L^m R^m \end{pmatrix} \begin{pmatrix} U_0 \\ U_b \\ U_m \end{pmatrix}, \quad (7)$$

where U_0 is the common ghost-free model used together with individual ghost-free models, U_b and U_m, to fit both the baseline and monitor data, respectively. With this formula, we can deghost the common events in both vintages consistently while preserving the difference between the two vintages in the individual ghost-free models. To maximize the deghosting consistency, we prioritize the inversion to obtain a common model, U_0, to fit both baseline and monitor data as much as possible.

Synthetic data example

We first tested our algorithm using 2D synthetic data with receiver ghost only. The baseline modeling used the original Sigsbee 2A model, whereas the monitor modeling used a modified Sigsbee 2A model with two 4D events in the deep section (Figure 1). The receiver depths of the baseline and monitor data were 30 ft and 50 ft, respectively.

Figures 2a and 2b show a shot gather for the baseline and monitor, respectively. Figures 2c and 2e show the zoom-in of the blue boxes in 2a and 2b, respectively. The wavelets of the baseline and monitor data were different due to different receiver depths. Figures 2d and 2f show the modeled data without ghost for Figures 2c and 2e, respectively.

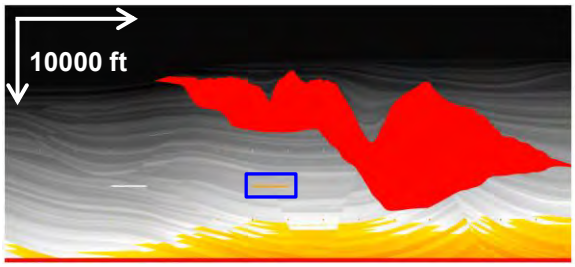

Figure 1: Sigsbee 2A model with two 4D events below sediment and salt, respectively. Blue box marks the target 4D event.

Figure 3a shows the spectral comparison of the baseline and monitor data before and after separate deghosting. The amplitude spectra of both data before deghosting (solid lines) were very different due to the different receiver depths. The amplitude spectra became similar after separate receiver deghosting (dashed lines). However, there were some residual ghost notches for both data. On the other hand, joint deghosting provided more accurate ghost removal for both data and thus a better match of the deghosted baseline (Figure 3b, dashed red line) and monitor data (Figure 3b, dashed blue line).

Figure 4 shows the migration differences between the baseline and monitor data around the target 4D event below the salt (Figure 1, blue box). We used the original Sigsbee 2A model to migrate both baseline and monitor data. This rendered kinematic errors below the target event in the monitor data. Not surprisingly, we observed similarly large 4D differences below the target event using the input baseline and monitor data from no-ghost modeling (Figure 4a), after separate deghosting (Figure 4b), and after joint deghosting (Figure 4c). We observed that, compared to separate deghosting (Figure 4b), joint deghosting (Figure 4c) provided a smaller difference above the target event where, theoretically, no 4D difference was expected (Figure 4a). Figure 4d shows the 4D error between the 4D difference of joint deghosting (Figure 4c) and the ground truth (Figure 4a).

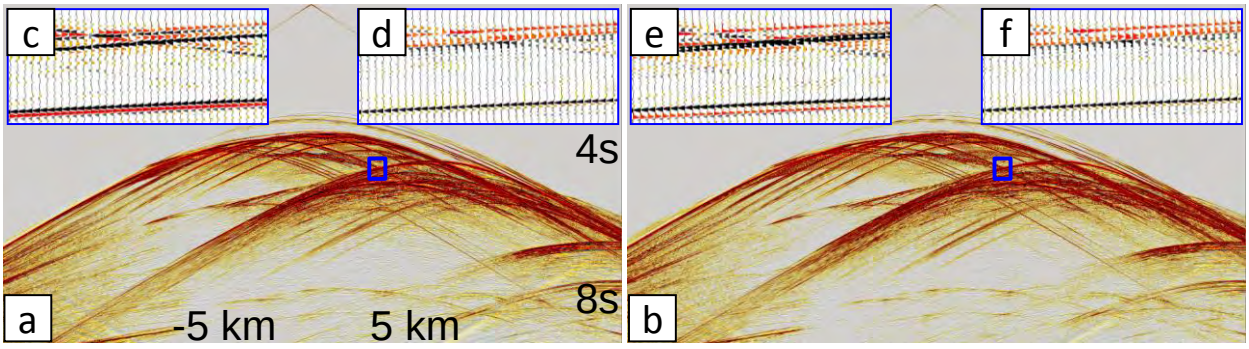

Figure 2: Modeled synthetic shot gather using (a) the Sigsbee 2A model with a receiver depth of 30 ft and (b) a modified Sigsbee 2A model with a receiver depth of 50 ft. (c) Zoom-in of the blue box in (a). (d) Zoom-in of the blue box in (a) without receiver ghost. (e) Zoom-in of the blue box in (b). (f) Zoom-in of the blue box in (b) without receiver ghost.

DOI http://dx.doi.org/10.1190/segam2015-5838448.1

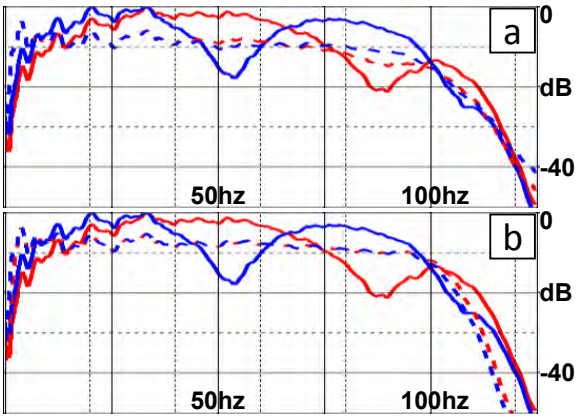

Figure 3: Spectral comparison before and after (a) separate deghosting and (b) joint deghosting. Red is the baseline, and blue is the monitor; solid lines are before deghosting, and dashed lines are after deghosting.

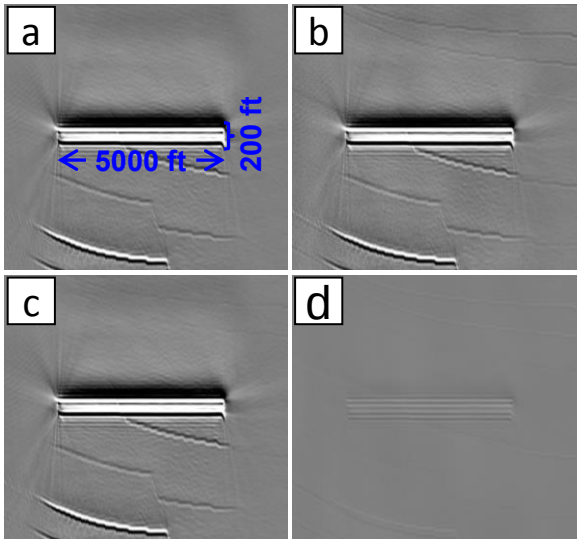

Figure 4: Migration differences between the baseline and monitor data: (a) Ground truth from no-ghost modeling, (b) after separate deghosting, and (c) after joint deghosting. (d) 4D error: (a)-(c).

Field data example

Next, we tested our algorithm on two narrow-azimuth (NAZ) surveys from the Santos Basin, Brazil. The baseline survey used eight streamers towed at 9 m (Figure 5, top), and the monitor survey used ten variable-depth streamers with receiver depths ranging between 8 m and 52 m (Figure 5, bottom). Both surveys had a nominal cable spacing of 100 m and channel spacing of 12.5 m. The shot depths of both surveys were 6 m. We did not expect significant geological changes because the two surveys were acquired only a few months apart.

The red lines (baseline) and yellow lines (monitor) in the middle of Figure 5 are the map-view of the receiver locations. The difference in the receiver locations of both vintages effectively improved the spatial sampling providing the potential for a more accurate plane-wave decomposition and better deghosting during joint 3D deghosting inversion.

Figures 6a and 6b show baseline and monitor shot gathers, respectively. Figures 6c and 6d are zoomed-in views of the blue boxes in Figures 6a and 6b, respectively. The water bottom wavelets were very different because of the different receiver profiles.

Figures 7a and 7b show the baseline and monitor gathers after separate 3D deghosting, respectively. The deghosted baseline and monitor data are closer to each other compared to the input data before deghosting (Figures 6a and 6b). However, apparent differences can still be identified (blue circles). The red arrows in Figure 7b point to some ringing artifacts, which are consistent with the residual ghost notch in the amplitude spectrum (Figure 7c, red arrow). The ringing artifacts become weaker after joint 3D deghosting (Figure 7e), and the data are more similar to each other after joint 3D deghosting (Figures 7d and 7e) compared to separate 3D deghosting (Figures 7a and 7b). Figure 7f indicates that joint 3D deghosting better removes the ghosts in both data (flatter spectra at ghost notches), and their spectra are better matched.

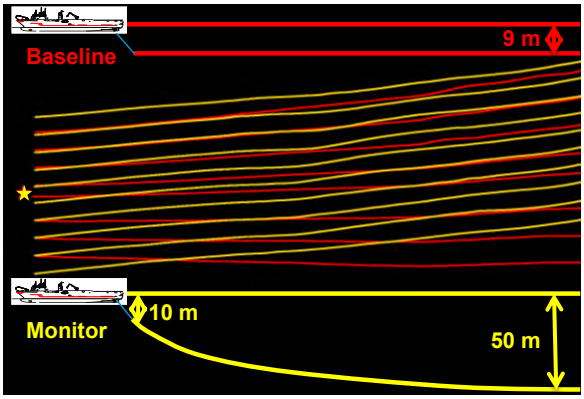

Figure 5: Top: Side-view of the cable profile of baseline survey. Bottom: Side-view of the cable profile of monitor survey. Middle: Map-view of receiver locations for baseline (red) and monitor (yellow) surveys. Stars represent shot locations of both surveys.

Conclusions and discussion

We demonstrated that joint 3D deghosting of baseline and monitor data provides more accurate deghosting and a more reliable 4D difference. The success is due to (1) better spatial sampling, (2) better full-bandwidth S/N due to ghost-notch diversity, and (3) consistent deghosting of common events while preserving the differences.

DOI http://dx.doi.org/10.1190/segam2015-5838448.1

The algorithm assumes the ghost-free wavefields from baseline and monitor data match each other before the joint deghosting inversion. Therefore, its success relies on how well we can perform water column correction, source designature/debubbling, and amplitude normalization. In the presence of strong noise, like any other deghosting process, joint deghosting inversion may significantly amplify the noise, which is not good for 4D analysis. In this case, a better strategy may be to perform joint 3D deghosting of baseline and monitor data and then reghost both ghost-free data using the same receiver depth to suppress the noise amplification.

The algorithm proposed here for joint 3D receiver deghosting of baseline and monitor towed-streamer data can be readily extended for joint 3D source deghosting of baseline and monitor OBN data. It can also be extended for joint 3D regularization of baseline and monitor data for both towed-streamer and OBN acquisition geometries.

Acknowledgments

We thank Chi Chen and Bing Bai for preparation of the field data. We also thank CGG for permission to present this work and the sponsors of the SMAART project for the Sigsbee 2A velocity model. Special thanks go to Jerry Young for encouragement and discussions.

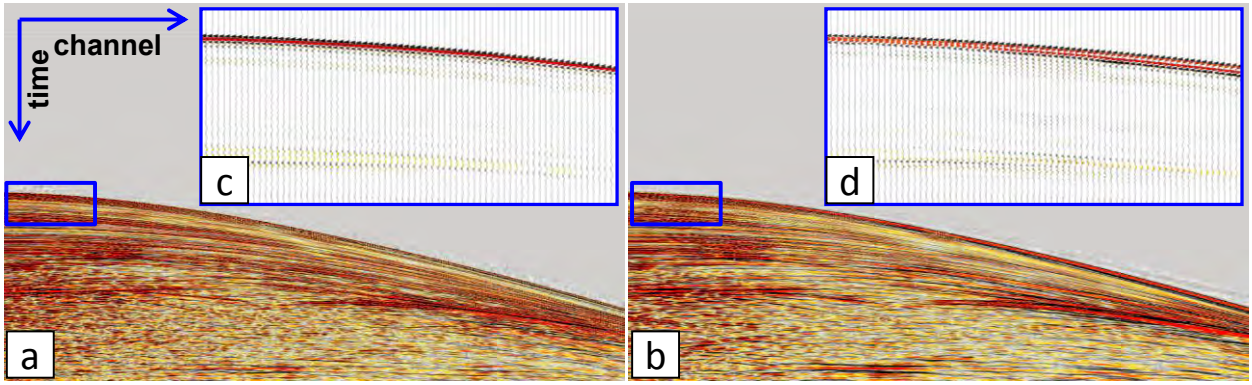

Figure 6: (a) Baseline and (b) monitor shot gathers before deghosting. (c) and (d) are zoom-ins of the blue boxes in (a) and (b), respectively, which highlight the difference in the water-bottom wavelets caused by different receiver depths.

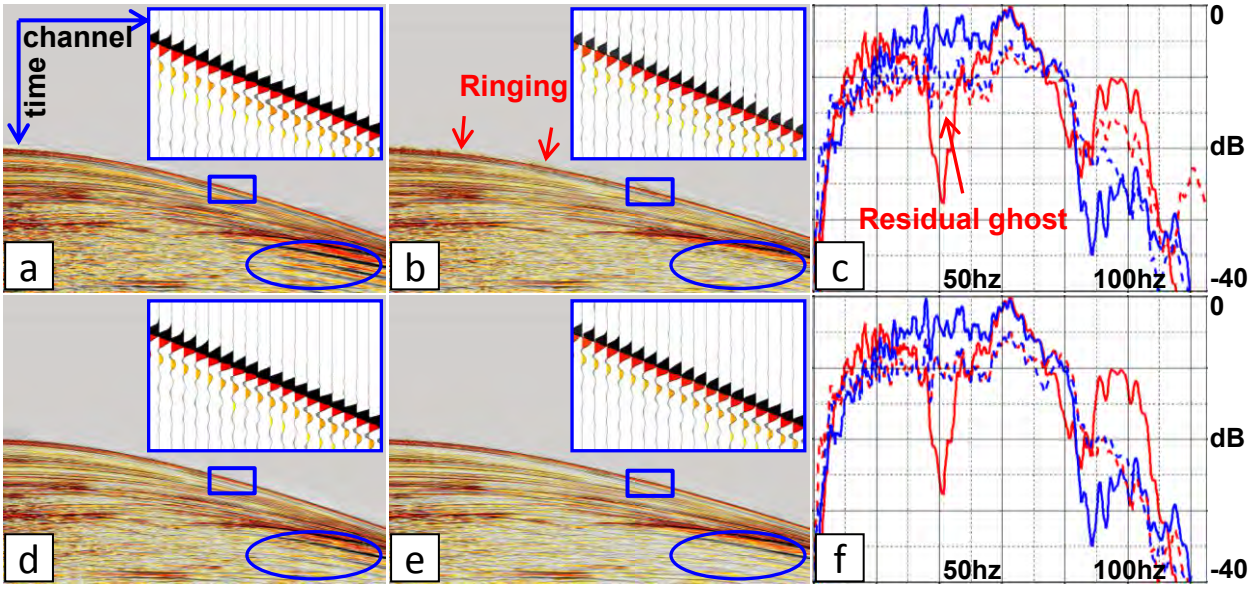

Figure 7: (a) Baseline and (b) monitor shot gathers after separate deghosting. (d) Baseline and (e) monitor gathers after joint deghosting. Spectral comparison before and after (c) separate deghosting and (f) joint deghosting. Blue is the baseline, and red is the monitor; solid lines are before deghosting, and dashed lines are after deghosting. The red solid lines in (c) and (f) indicate that the variable-depth data have better low frequency signals than flat-towed data due to the deeper receiver depth.

DOI http://dx.doi.org/10.1190/segam2015-5838448.1

EDITED REFERENCES

Note: This reference list is a copyedited version of the reference list submitted by the author. Reference lists for the 2015 SEG Technical Program Expanded Abstracts have been copyedited so that references provided with the online metadata for each paper will achieve a high degree of linking to cited sources that appear on the Web.

REFERENCES

Carlson, D., A. Long, W. Sollner, H. Tobti, R. Tenghamn, and N. Lunde, 2007, Increased resolution and penetration from a towed dual-sensor streamer: First Break, **25**, 71–77.

Hicks, E., H. Hoeber, G. Poole, and B. King, 2014, An efficient 4D processing flow for variable depth streamer data: The Leading Edge, **33**, 172–180. http://dx.doi.org/10.1190/tle33020172.1.

Özdemir, A., R. Caprioli, P. Özbek, A. Kragh, and J. Robertsson, 2008, Optimized deghosting of over/under towed-streamer data in the presence of noise: The Leading Edge, **27**, 190–199. http://dx.doi.org/10.1190/1.2840366.

Poole, G., 2013, Pre-migration receiver de-ghosting and re-datuming for variable depth streamer data: 83rd Annual International Meeting, SEG, Expanded Abstracts, 4216–4220.

Poole, G., C. Davison, J. Deeds, K. Davies, and G. Hampson, 2013, Shot-to-shot directional designature using near-field hydrophone data: 83rd Annual International Meeting, SEG, Expanded Abstracts, 4236–4240.

Riyanti, C. D., R. G. van Borselen, P. M. van den Berg, and J. T. Fokkema, 2008, Pressure wavefield deghosting for non-horizontal streamers: 78th Annual International Meeting, SEG, Expanded Abstracts, 2652–2656.

Robertsson, J., I. Moore, M. Vassallo, A. K. Özdemir, D. J. van Manen, and A. Özbek, 2008, On the use of multicomponent streamer recordings for reconstruction of pressure wavefields in the crossline direction: Geophysics, **73**, no. 5, A45–A49. http://dx.doi.org/10.1190/1.2953338.

Van der Schans, C. A., and A. M. Ziolkowski, 1983, Angular-dependent signature deconvolution: 53rd Annual International Meeting, SEG, Expanded Abstracts, 433–435.

Wang, P., K. Nimsaila, D. Zhuang, Z. Fu, H. Shen, G. Poole, and N. Chazalnoel, 2015, Joint 3D source-side deghosting and designature for modern air-gun arrays: Presented at the 77th Annual International Conference and Exhibition, EAGE.

Wang, P., S. Ray, and K. Nimsaila, 2014, 3D joint deghosting and crossline interpolation for marine single-component streamer data: 84th Annual International Meeting, SEG, Expanded Abstracts, 3594–3598.

Ziolkowski, A., G. E. Parkes, L. Hatton, and T. Haugland, 1982, The signature of an air gun array: Computation from near-field measurements including interactions: Geophysics, **47**, 1413–1421. http://dx.doi.org/10.1190/1.1441289.

DOI http://dx.doi.org/10.1190/segam2015-5838448.1